

# Cooperative C-O Bond Activation by a Heterobinuclear Al-Fe Complex Operating by a Radical Pair Mechanism

Soumen Sinhababu<sup>†</sup>, Maxim R. Radzhabov<sup>†</sup>, and Neal P. Mankad<sup>\*</sup>

Department of Chemistry, University of Illinois at Chicago, 845 W. Taylor St., Chicago, Illinois 60607, United States

**ABSTRACT:** Activation of inert molecules like CO<sub>2</sub> is often mediated by cooperative chemistry between two reactive sites within a catalytic assembly, the most common form of which is Lewis acid/base bifunctionality observed in both natural metalloenzymes and synthetic systems. Here, we disclose a heterobinuclear complex with an Al-Fe bond that instead activates CO<sub>2</sub> and other substrates through cooperative behavior of two radical intermediates. The complex L(Me)Al-Fp (**2**, L = HC{(CMe)(2,6-<sup>i</sup>Pr<sub>2</sub>C<sub>6</sub>H<sub>3</sub>N)}<sub>2</sub>, Fp = FeCp(CO)<sub>2</sub>) was found to insert CO<sub>2</sub> and cyclohexene oxide, producing LAl(Me)(μ:κ<sub>2</sub>-O<sub>2</sub>C)Fp (**3**) and LAl(Me)(μ-OC<sub>6</sub>H<sub>10</sub>)Fp (**4**), respectively. Further atom transfer, decarbonylation, and isomerization reactivity was also observed. Detailed mechanistic studies on the CO<sub>2</sub> and epoxide insertion reactions indicate an unusual mechanism in which (i) the Al-Fe bond dissociates homolytically to generate formally Al<sup>II</sup> and Fe<sup>I</sup> metalloradicals, then (ii) the metalloradicals add to substrate in a pairwise fashion initiated by O-coordination to Al. The accessibility of this unusual mechanism is aided, in part, by the redox non-innocent nature of L that stabilizes formally Al<sup>II</sup> intermediates with predominantly Al<sup>III</sup>-like character. This “radical pair” pathway represents an unprecedented mechanism for CO<sub>2</sub> activation.

## INTRODUCTION

Identifying new reaction pathways for activation of inert substrates enables rational design of catalysts for challenging synthetic transformations. Although historically the activation of inert substrates by coordination complexes has focused on unsaturated mononuclear systems with single-site reactivity, recently there has been a resurgence in cooperative bond activation studies in which reactivity is delocalized over two or more reactive sites within a well-defined system. Examples include frustrated Lewis pairs (FLPs),<sup>1</sup> metal-ligand bifunctional catalysts,<sup>2</sup> homo- and heterobinuclear metal complexes,<sup>3</sup> and multinuclear metal clusters.<sup>4</sup> As a representative example, one can consider the coordination chemistry of CO<sub>2</sub>. While CO<sub>2</sub> activation by mononuclear metal complexes has been mapped extensively,<sup>5</sup> remaining challenges in catalytic CO<sub>2</sub> fixation have motivated numerous studies on cooperative CO<sub>2</sub> activation.<sup>6</sup> The dominant paradigm is one of Lewis acid/base bifunctionality (Figure 1a): a Lewis basic reactive site adds a reactive electron pair to the carbon center of CO<sub>2</sub>, while the resultant buildup of negative charge on oxygen is simultaneously stabilized by a Lewis acidic reactive site.<sup>7</sup> Since the seminal work of Floriani on cooperative CO<sub>2</sub> activation by low-valent Co/M bifunctional systems (M = alkali metal),<sup>8</sup> numerous examples of metal- and non-metal-based systems functioning by this paradigm have been identified.<sup>9</sup> Moreover, Lewis acid/base bifunctionality is thought to be the operative paradigm in nature, stabilizing CO<sub>2</sub>-activated intermediates in both aerobic (Mo/Cu) and anaerobic (Ni/Fe) carbon monoxide dehydrogenase enzymes.<sup>10</sup> Identifying reaction pathways beyond this prevailing CO<sub>2</sub> activation manifold has the potential to open new catalyst design strategies.<sup>11</sup>

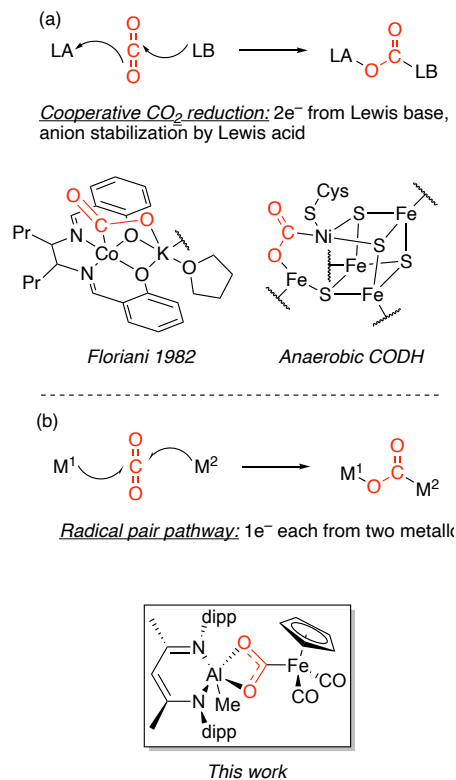
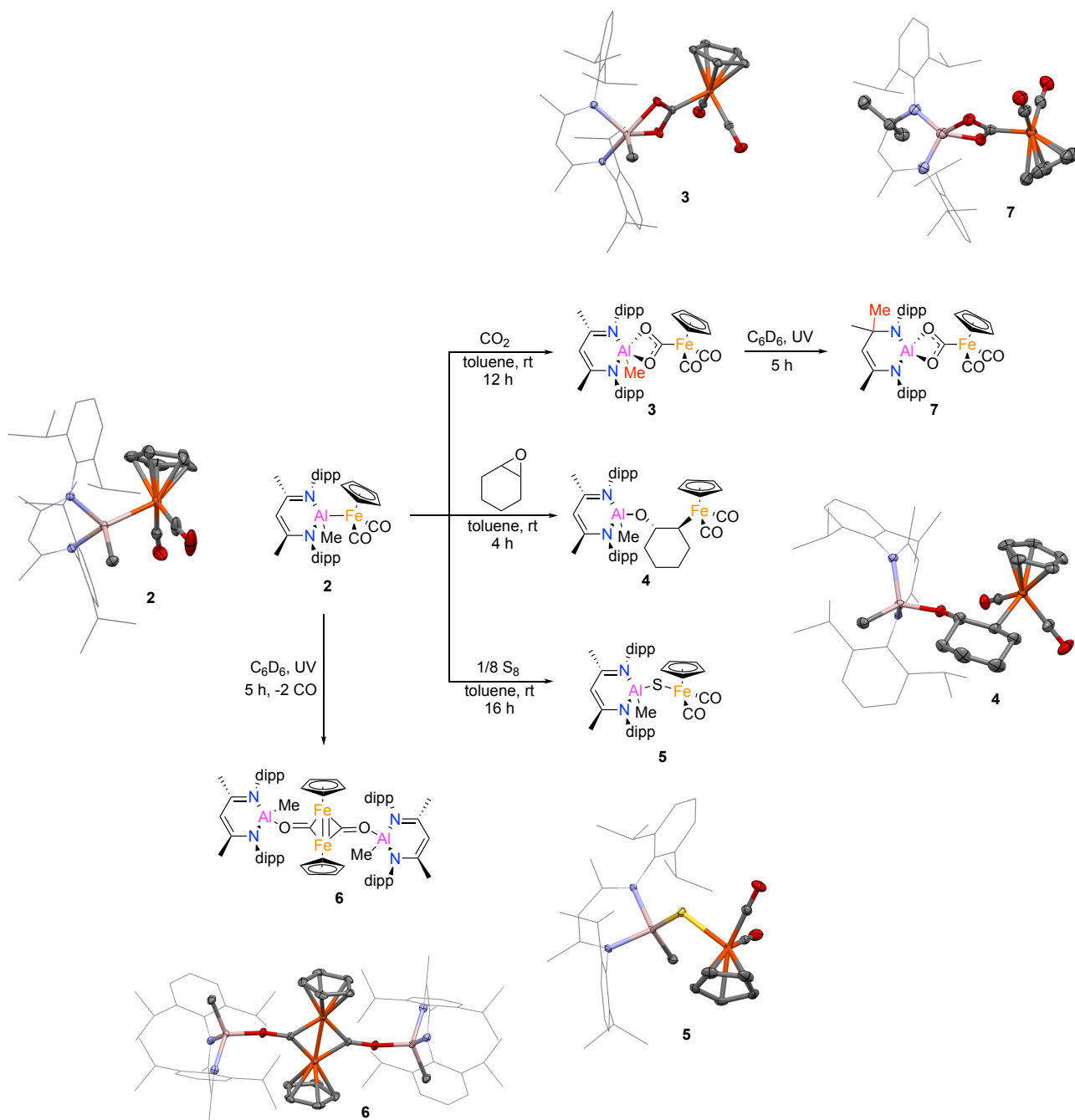


**Figure 1.** Cooperative CO<sub>2</sub> activation pathways and representative examples: (a) Lewis acid/base bifunctionality, (b) radical pair chemistry (this work).

In this report, we disclose a system that activates CO<sub>2</sub> and other substrates by a radical pair mechanism, which is a novel mechanistic paradigm for cooperative CO<sub>2</sub> reactivity (Figure





**Scheme 1.** Thermal and photochemical reactivity studies of an Al<sup>III</sup>-Fe heterobinuclear system, including solid-state structures of complexes 2-7 determined by X-ray crystallography. For clarity, hydrogen atoms and co-crystallized solvent molecules are omitted from the crystal structures; ligand backbones (except nitrogen) are shown as wireframes, and all other atoms are shown as 50% probability ellipsoids.

The molecular structures of **2** and **4** feature four-coordinate aluminum centers with distorted tetrahedral geometries, while **3** has a penta-coordinate aluminum center with distorted square pyramidal geometry, as determined by X-ray crystallography. The Fe-Al bond length [2.478(9) Å] in **2** is comparable to the value of 2.480(1) Å reported for the related compound LAl(Cl)Fp\* (Fp\* = Cp\*Fe(CO)<sub>2</sub>; Cp\* = C<sub>5</sub>Me<sub>5</sub>).<sup>22c</sup> The Al-O bond lengths in **3** [1.980(1) and 1.897(1) Å] are slightly longer to the corresponding bonds [1.880(5) and 1.861(4) Å] present in (NON)Al(κ<sub>2</sub>-O<sub>2</sub>C)AuP<sup>t</sup>Bu<sub>3</sub> (NON = 4,5-bis(2,6-diisopropyl-anilido)-2,7-di-tert-butyl-9,9-dimethylxanthene) reported by

the Aldridge group,<sup>24</sup> possibly due to the different aluminum oxidation states. The O-C bond lengths for the Al(κ<sub>2</sub>-O<sub>2</sub>C)Fe unit in **3** [1.271(2) and 1.298(2) Å] fall between the typical ranges for C-O single and double bonds. The Fe-C bond [1.933(1) Å] of the Al(κ<sub>2</sub>-O<sub>2</sub>C)Fe unit is considerably longer than the Fe-C bond [1.87(1) Å] seen in Ph<sub>3</sub>Sn(κ<sub>2</sub>-O<sub>2</sub>C)FeCl(depe)<sub>2</sub> (depe = 1,2-bis(diethylphosphino)ethane).<sup>27</sup> The molecular structure of **4** reveals that LAl(Me)O and Fp moieties are in *trans* orientation about the cyclohexane unit. The Al-O bond length [1.728(2) Å] is quite shorter than those

in compound **3**. The Fe-C<sub>cy</sub> bond length is 2.111(3) Å, which is in range of reported Fe-C<sub>alkyl</sub> bonds.<sup>28</sup>

Complex **2** was also found to do sulfur atom abstraction from elemental sulfur, giving product **5** in which sulfur inserted into the Al-Fe bond (64%, Scheme 1). As expected, the Al-S bond length in **5** determined by X-ray crystallography [2.2005(7) Å] is longer than the Al=S bond length [2.104(1) Å] present in LAI=S(NHC) (NHC = [{(CH<sub>2</sub>)CN(Pr)}<sub>2</sub>C])<sup>29</sup> but close to Al-S single bonds in [LAl(μ-S)<sub>2</sub>TiCp<sub>2</sub>] (2.208(1) and 2.197(1) Å).<sup>30</sup> The Fe-S bond distance (2.3161(8) Å) is in the range of those reported in related organoiron-sulfur complexes (2.26-2.35 Å).<sup>31</sup>

**Photochemical reactivity:** Complexes **2** and **3** are stable thermally (up to 60 °C) in C<sub>6</sub>D<sub>6</sub> for at least for 12 h but were found to react further upon irradiation with UV light. Irradiation of a C<sub>6</sub>D<sub>6</sub> solution of **2** for 5 h at room temperature resulted in yellow crystals of new complex **6** in low yield (Scheme 1). The solid-state IR spectrum of **6** does not show any intense bands in the 2100-1800 cm<sup>-1</sup> region characteristic of terminal carbonyl groups, but a new band indicative of bridging carbonyl groups was observed at 1524 cm<sup>-1</sup>. Due to poor solubility in common organic solvents, we could not characterize complex **6** in the solution state, but the identity of the product was confirmed by single-crystal XRD studies. The molecular structure consists of two [LAl(Me)] and one [(CpFeCO)<sub>2</sub>] motifs. It is worth mentioning here that the [(CpFeCO)<sub>2</sub>] motif was not characterized structurally in any complex to date, despite the long history of [CpFe(CO)<sub>2</sub>]<sub>2</sub> chemistry.<sup>32</sup> The Fe-Fe distance in **6** is 2.3543(5) Å, which is significantly shorter than the Fe-Fe single bond of the classical [Fe<sub>2</sub>(CO)<sub>9</sub>] [2.523(1) Å] or in [CpFe(CO)<sub>2</sub>]<sub>2</sub> [2.5389(3) Å] and thus can be formulated as a Fe=Fe double bond.<sup>33,34</sup> The C-O bond length in **6** [1.292(3) Å] is longer than the terminal C-O bonds [1.157(4) Å] present in **2**.

Subsequently, a C<sub>6</sub>D<sub>6</sub> solution of **3** was irradiated at ambient temperature for 5 h. The <sup>1</sup>H NMR spectrum reveals complete conversion of **3** to **7** (Scheme 1). In the <sup>1</sup>H NMR spectrum of

compound **3**, the methyl protons bonded to the aluminum center appear as a singlet at -0.20 ppm but are shifted downfield to 1.71 ppm in **7**, indicating methyl migration from the aluminum center to the ligand backbone. The crystal structure of **7** revealed that its aluminum center is tetra-coordinate with two nitrogen and two oxygen atoms in its immediate environment. It also confirmed that the methyl group migrated from aluminum to the β-diketimate backbone as anticipated from <sup>1</sup>H NMR spectroscopy. The methyl migration to the β-diketimate ligand and transforms it into a dianionic ligand. Although the M-C bond migration phenomenon is common in transition metal β-diketimate chemistry, this is first report involving an aluminum β-diketimate.<sup>35</sup> The C<sub>3</sub>N<sub>2</sub>Al six membered ring is puckered with both Al-N bonds being almost equal in distance [1.774(3) Å and 1.808(3)]. The Al-O bond lengths [1.862(2) Å and 1.848(2)] are shorter than in **3** due to change in coordination number at the aluminum center.

**Computational analysis of atomic charges & bonding.** To better understand the origins of reactivity of our Al<sup>III</sup>-Fe heterobimetallic complex LAI(Me)Fp (**2**), we decided to study the charge distribution using NBO<sup>36</sup> (Figure S19) and QTAIM<sup>37</sup> (Figure 3) analysis methods on pre-optimized geometries for complex **2** and, for modelling purposes, its simplified counterparts with methyl (Me) **8** and phenyl (Ph) **9** substituents in place of 2,6-diisopropylphenyl (dipp) in **2**. QTAIM charges, being origin-independent<sup>38</sup> and more “chemically intuitive”, are consistent with representation of complexes **2**, **8** and **9** as featuring strongly polarized covalent Al<sup>III</sup>-Fe<sup>0</sup> bonds. For comparison, we also calculated NBO and QTAIM charges for a well-studied heterobimetallic system,<sup>39</sup> Me<sup>i</sup>MesCuFp **10** (Me<sup>i</sup>MesMes = 1,3-bis(2,4,6-trimethylphenyl)-4,5-dimethylimidazol-2-ylidene, Figures S19 and 3). Just like for Al-Fe complexes, QTAIM charges are much closer to traditional ideas of valences, with Cu being in the oxidation state of (almost) one and Fe being in the oxidation state of zero.

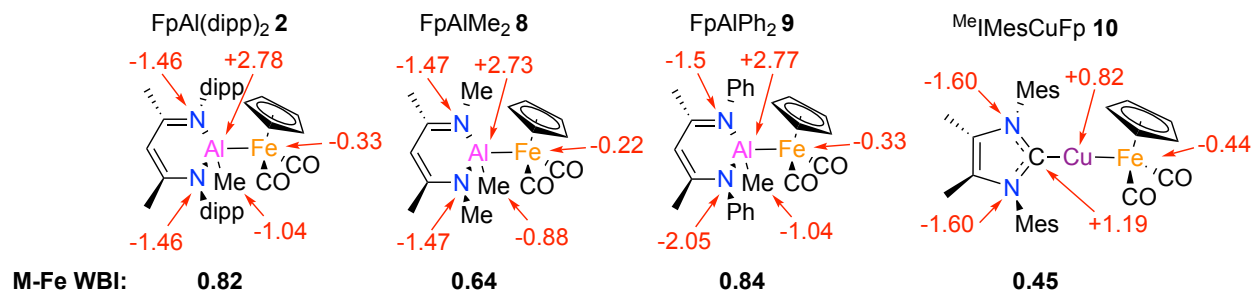


**Figure 3.** Calculated QTAIM charges for selected atoms in **2** and **8-10**, with M-Fe Wiberg bond indices indicated below the structures.

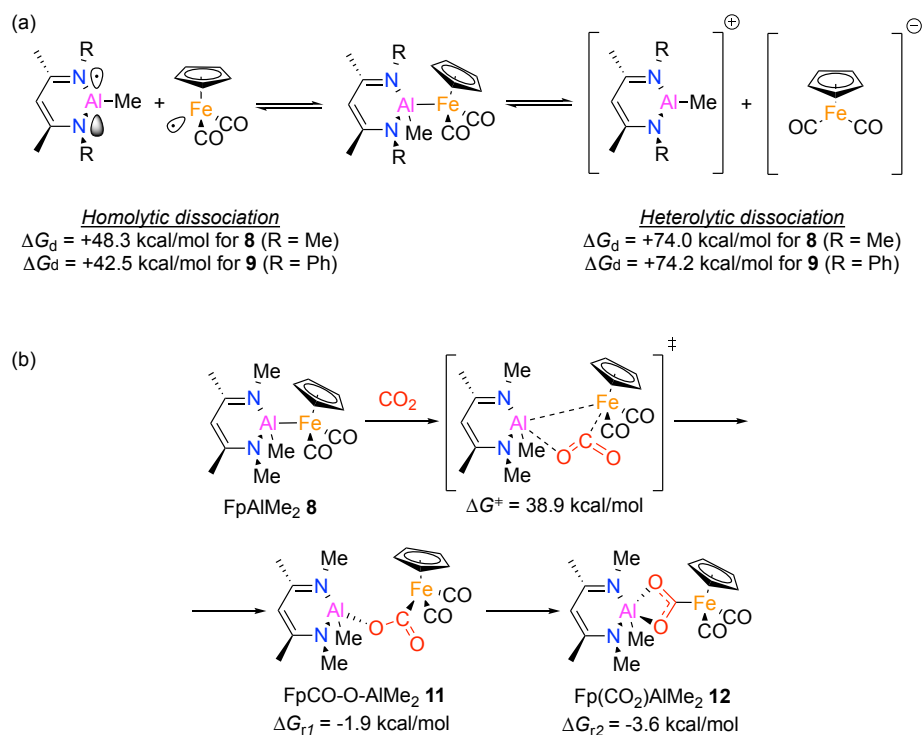
To further confirm the presence of the covalent bond between two metals, we calculated Wiberg Bond Indices (WBI) in Löwdin orthogonalized basis<sup>40</sup> (Figure 3 and Table S1). From the obtained data we can conclude that the Al-Fe bond in **2** is almost twice as covalent as the Cu-Fe bond in **10**.

Although the used methods gave quite differing charge values, trends between structures in question are consistent. This allowed us to (initially) simplify our model and study Me-substituted complex **8** in lieu of complex **2** to study its reactivity *in silico* towards CO<sub>2</sub> insertion and epoxide ring opening at a lower computational cost.

**Combined computational/experimental investigation of reaction mechanisms.** We decided to begin with calculating

energies for two dissociation pathways (Scheme 2a), homolytic and heterolytic, for truncated model complexes **8** and **9**. However, dissociation energies for both **8** and **9** proved to be too high, even when including effects of the toluene solvent. It is worth noting that Gibbs free energies and enthalpies are significantly (>20 kcal/mol) lower for homolytic rather than heterolytic dissociation. Steric bulkiness of substituents (i.e. Me vs Ph) appeared rather irrelevant: for homolytic dissociation both ΔG<sub>d</sub> and ΔH<sub>d</sub> were just ~6 kcal/mol lower for significantly bulkier Ph (**9**), and for heterolytic dissociation Gibbs free energies and enthalpies for Ph were even higher than for Me (**8**). Therefore, we decided not to proceed with dissociation calculations

for complex **2** (R = dipp), a decision that later proved imprudent.



**Scheme 2.** Unscaled Gibbs free energies (PBE1PBE) for (a) Al-Fe bond dissociation and (b) concerted CO<sub>2</sub> insertion pathways.

Since calculated dissociation energies turned out to be too high for reactions that occur readily at ambient conditions, we decided to explore possible mechanistic pathways beginning with the concerted CO<sub>2</sub> insertion (Scheme 2b) via the corresponding transition state (TS). Obtained Gibbs free energies (all relative to **8**) indicated that while the CO<sub>2</sub> insertion *per se* is thermodynamically favorable, the concerted pathway's high activation barrier is inconsistent with a reaction that occurs with reasonable rate at room temperature, which is what was observed experimentally. To make sure the obtained TS energy was not some sort of a functional artifact, we recalculated the transition state energy using several DFT functionals (Figure S16), as well as the TS energy of CO<sub>2</sub> insertion for complex **9**. Obtained Gibbs free energies are generally consistent among all employed functionals, which indicates that such a high obtained value is not an error of the chosen functional.

However, it is commonly accepted<sup>41</sup> that translational entropies for reactions in solution should be corrected (scaled) since the loss of molar entropy when two or more molecules in solution interact is not accounted by solvation free energies. Thus, we applied one of the most used correction methods,<sup>42</sup> which effectively calls for neglecting the contribution of translational entropy altogether. Since such an approach introduces an unknown degree of uncertainty to the Gibbs energies, we limited ourselves only to qualitative comparison of the calculated activation barriers. The scaled TS Gibbs energies (Figure S16) were found to be in the desired range ( $\sim 25 \pm 1$  kcal/mol) for some functionals. Nevertheless, the activation barrier for this reaction would be higher since the real translational entropy term is not zero.

To gain additional insights on the mechanism, we next conducted an Eyring analysis by obtaining experimental, pseudo-

first order (excess CO<sub>2</sub>) rate constants for CO<sub>2</sub> activation by **2** across the temperature range 263-303 K (Figure 4). Fitting the data to the Eyring equation provided the experimentally determined activation parameters for CO<sub>2</sub> insertion by complex **2**:  $\Delta H^\ddagger = 24.9$  kcal/mol,  $\Delta S^\ddagger = 20.5$  kcal/mol\*K,  $\Delta G^\ddagger_{298K} = 18.8$  kcal/mol. The activation entropy for this reaction is large and positive, which indicates a dissociative rate-determining step and is therefore inconsistent with the concerted mechanism shown in Scheme 2b (which should give  $\Delta S^\ddagger < 0$ ). Moreover, the *trans*-stereochemistry of the ring-opened product **4** evident by X-ray crystallography indicates *anti*-addition of the two metals to the epoxide and thus also testifies against any similar concerted mechanisms.

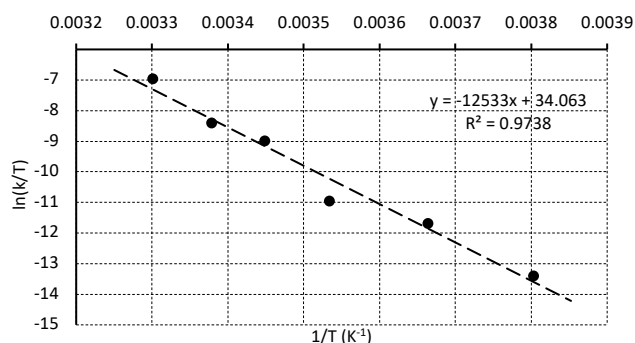
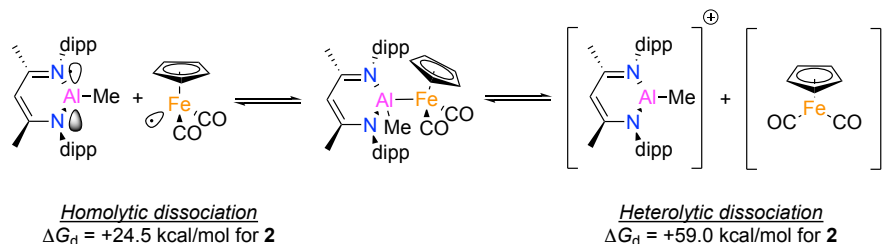


**Figure 4.** Eyring analysis to extract activation parameters for the CO<sub>2</sub> activation reaction by **2**.

With these considerations in mind, we decided to revisit the dissociation pathways, this time with the model for **2** with full-sized dipp-substituted ligands (Scheme 3). To our surprise, the dissociation Gibbs free energies and enthalpies were  $\sim 15$

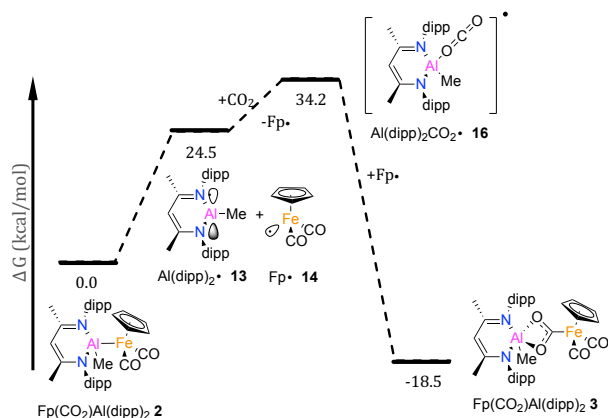
kcal/mol lower than for closest counterpart **9**. This brought the activation barrier down, closer to the experimental value and within the expected range for a room-temperature reaction. Therefore, *relying on models with truncated substituents, a common approach in computational organometallic chemistry, is not always justified*. It is curious that addition of just two

isopropyl groups to each phenyl ring had such drastic effect on dissociation energies, which we attribute solely to significantly higher steric tension in complex **2** relative to **8** and **9**, given their similar electronic structures. Collectively, these observations also reinforce *the critical importance of calibrating computed mechanisms with experimental (preferably kinetics) data*.



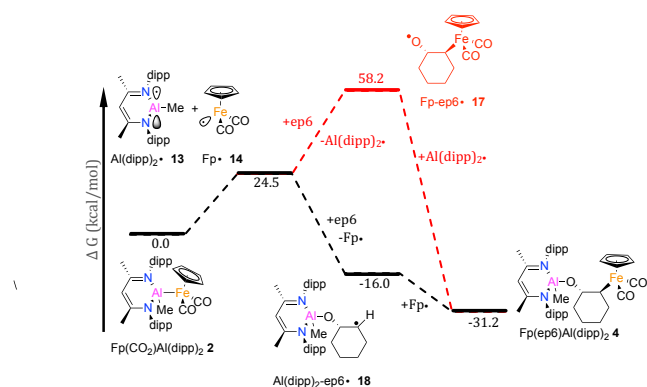
**Scheme 3.** Gibbs free energies (PBE1PBE) for Al-Fe bond dissociation of **2**;

With more evidence towards homolytic dissociation of complex **2** as the origin of its reactivity and having ruled out several alternatives (Figure S18), we calculated the Gibbs free energies of interactions of both Al and Fe metalloradicals with both CO<sub>2</sub> and cyclohexene oxide. As follows from the obtained Gibbs energies, it is clear that both CO<sub>2</sub> and cyclohexene oxide prefer to react with the Al radical **13** (Al(dipp)<sub>2</sub>) first rather than with Fe radical **14** (Fp), as indicated in Scheme 4. In the first case, for CO<sub>2</sub> insertion, we could not localize a minimum corresponding to the radical Fe-CO<sub>2</sub> complex **15** (however, we were able to localize a minimum for a similar anionic complex, which has been observed experimentally<sup>43</sup>; see SI for more details). Instead, the localized minimum was some sort of a supramolecular complex of Fp radical **14** and CO<sub>2</sub>, held together by weak non-covalent bonds (as shown by QTAIM diagrams and calculated WBIs; Figure 5a). However, we localized a minimum for the complex **16** where a linear CO<sub>2</sub> molecule is coordinated on the Al center of complex **13**, giving a quite strong covalent bond (also Figure 5a). Such coordination is endothermic, but the subsequent interception of Fp radical **14** makes CO<sub>2</sub> insertion a thermodynamically favorable process.

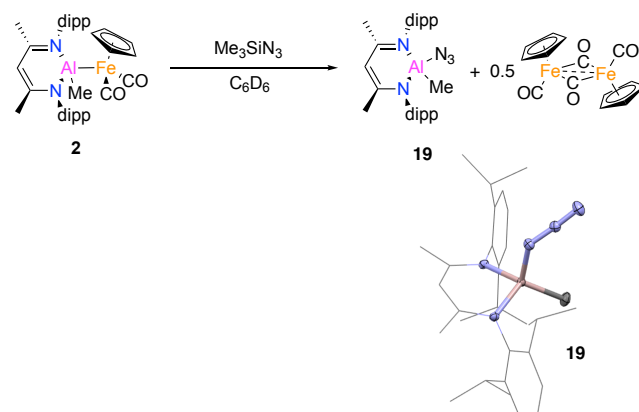


**Scheme 4.** Gibbs free energy diagram for calculated pathways of CO<sub>2</sub> activation mediated by **2**.

Epoxide ring opening is also an exothermic process even for initiation with the Al radical **13**, while initiation by Fe radical **14** has a very high barrier (Scheme 5). Subsequent recombination of Al-epoxide complex **18** with Fp **14** to give the observed product **4** is energetically very favorable.



**Scheme 5.** Gibbs free energy diagrams for calculated pathways of cyclohexene oxide ring opening mediated by **2**.



**Scheme 6.** Reaction of **2** and Me<sub>3</sub>SiN<sub>3</sub>, including solid-state structures of complex **19** determined by X-ray crystallography. For clarity, hydrogen atoms and co-crystallized solvent molecules are omitted from the crystal structures; ligand backbones (except nitrogen) are shown as wireframes, and all other atoms are shown as 50% probability ellipsoids.

The identification of the O-bound CO<sub>2</sub> adduct **16** along the reaction pathway is notable, as this coordination mode has rarely been observed experimentally<sup>44</sup> and is typically proposed

during (1-electron) reductive coupling of CO<sub>2</sub> to form oxalate<sup>45</sup> (rather than for 2-electron CO<sub>2</sub> reduction). Moreover, it is a rare example of a formally Al<sup>II</sup> species playing an important role in reactivity.<sup>46</sup> Thus, we chose to analyze the electronic structure of **16** and its precursor complex **13** further. Calculated Mulliken spin densities for selected atoms (Figure 5b) of these complexes indicate that the unpaired electron is mostly delocalized through the conjugated  $\beta$ -diketiminato ligand but not on Al itself for either complex, nor on the CO<sub>2</sub> moiety in the case of **16**. In other words, although **13** is formally a [(L<sup>-</sup>)Al<sup>II</sup>(Me)] species, it is perhaps better formulated as [(L<sup>2-</sup>)Al<sup>III</sup>(Me)] and thus possess a vacant Al-centered 3p<sub>z</sub> orbital for substrate coordination.

Given these computational results indicating an unusual radical-pair mechanism for the cooperative bond activation chemistry of **2**, we sought experimental evidence for formation of metalloradicals **13** and/or **14** under relevant conditions. One observation we can report is the reaction of **2** with excess Me<sub>3</sub>SiN<sub>3</sub>, which resulted LAI(Me)N<sub>3</sub> (**19**) and Fp<sub>2</sub> as major products (Scheme 6). The formation of Fp<sub>2</sub> as the dominant Fe-containing product in this reaction can be viewed as experimental validation of metalloradical **14** forming *in situ*. Further evaluation of the radical-pair reactivity of **2** is currently underway in our laboratory.

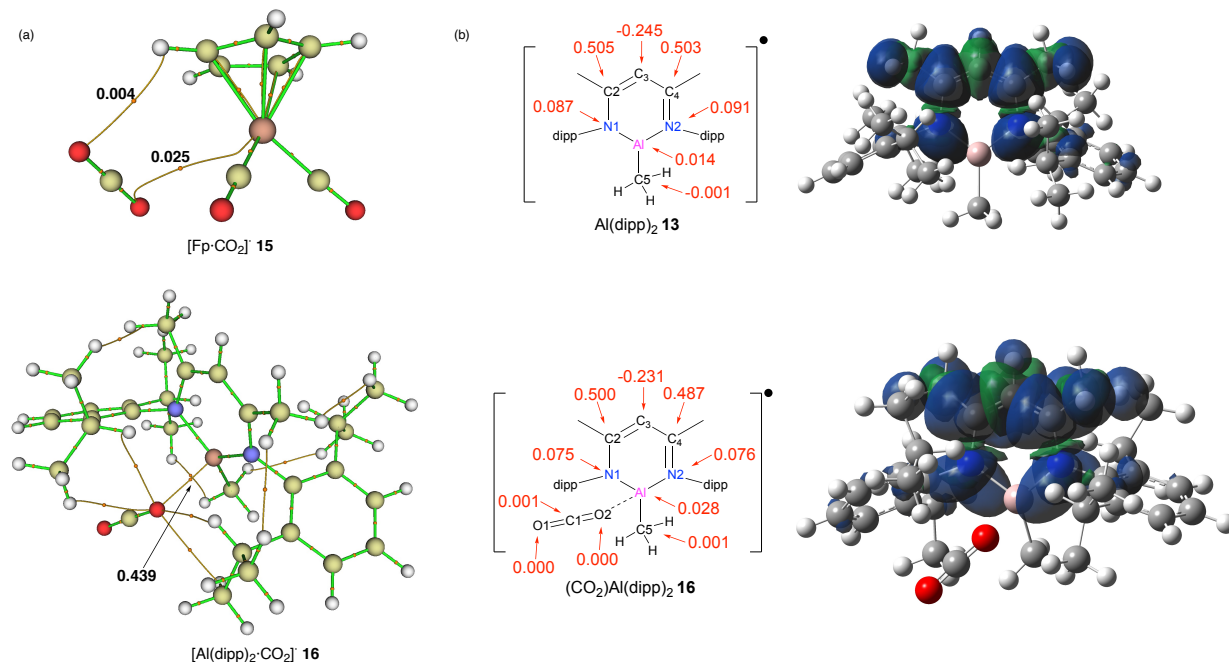


**Figure 5.** (a) Selected QTAIM paths connecting (3,-3) and (3,-1) critical points for **15** and **16** with key all-electron Wiberg bond indices shown; (b) calculated Mulliken spin densities for selected atoms and corresponding spin density plots for **13** and **16**.

## CONCLUSIONS

A series of reactivity studies were carried out on a heterobimetallic Al-Fe complex, **2**. Most notably, complex **2** reacts cleanly with CO<sub>2</sub> and cyclohexene oxide, giving CO<sub>2</sub> inserted product **3** and epoxide ring opening product **4**, respectively. Detailed kinetic and theoretical studies were performed on these two reactions and indicated an unusual radical-pair mechanism in which Al-Fe homolytic dissociation precedes pairwise metalloradical addition to substrate. Particularly novel aspects of this study include:

- Unexpected involvement of formally Al<sup>II</sup> reactive intermediates
- An unprecedented mechanism for CO<sub>2</sub> activation
- An instructive interplay between theory and experiment that emphasizes the importance in computational organometallic chemistry of (i) validating calculated reaction pathways with kinetics measurements, and (ii) modeling complete (as opposed to truncated) ligand substituents

## METHODS

**Experimental methods.** All experimental manipulations were carried out under inert dinitrogen atmosphere using standard Schlenk line and glovebox techniques. All new compounds were characterized by <sup>1</sup>H and <sup>13</sup>C{<sup>1</sup>H} NMR spectroscopy, solid-state IR spectroscopy, and single-crystal X-ray diffraction. Detailed experimental procedures and spectral data are available as Supplementary Information, and supporting crystallographic data in the form of CIF files are available upon request from the Cambridge Crystallographic Data Centre using deposition numbers 2100519-2100525.

**Computational methods.** Density Functional Theory calculations (at the PBE0<sup>47a</sup>-G3BJ<sup>47b</sup>/def2-TZVP<sup>47c</sup> level of theory; SMD<sup>47d</sup> solvation model with toluene parameters), as implemented in the Gaussian 16 (Revision B.01)<sup>48</sup> code, were employed to optimize molecular geometries and determine bonding energies, Mulliken spin densities and NBO charges (using NBO version 3.1,<sup>49</sup> as implemented in Gaussian 16). The open-source MultiWFN<sup>50</sup> (version 3.8) program was employed to calculate and visualize Wiberg bond indices, QTAIM charges, critical points and paths (using data derived from Gaussian DFT calculations). For more details on comprehensive computational methods please see Supplementary Information.

## ASSOCIATED CONTENT

## Supporting Information

The Supporting Information is available free of charge on the ACS Publications website.

Experimental procedures, spectral data, computational data (PDF)

## AUTHOR INFORMATION

### Corresponding Author

\* npm@uic.edu

### Author Contributions

†These authors contributed equally.

## ACKNOWLEDGMENT

This material is based upon work supported by the U.S. Department of Energy (DOE), Office of Science, Office of Basic Energy Sciences (BES), under Award Number DE-SC0021055. Computational resources and services were provided by the Advanced Cyberinfrastructure for Education and Research (ACER) group at UIC. Instrumentation for X-ray crystallography at UIC was funded, in part, by the National Institutes of Health under grant R01 GM116820. The structure of complex **7** was obtained using NSF's ChemMatCARS Sector 15 supported by the Divisions of Chemistry (CHE) and Materials Research (DMR), National Science Foundation, under grant number NSF/CHE-1834750. Use of the Advanced Photon Source, an Office of Science User Facility operated for the DOE Office of Science by Argonne National Laboratory, was supported by the U.S. DOE under Contract No. DE-AC02-06CH11357.

## REFERENCES

- (1) Stephan, D. W. The Broadening Reach of Frustrated Lewis Pair Chemistry. *Science* **2016**, *354*, 7229.
- (2) (a) Gunanathan, C.; Milstein, D. Metal–Ligand Cooperation by Aromatization–Dearomatization: A New Paradigm in Bond Activation and “Green” Catalysis. *Acc. Chem. Res.* **2011**, *44*, 588–602. (b) Morris, R. H. Exploiting Metal–Ligand Bifunctional Reactions in the Design of Iron Asymmetric Hydrogenation Catalysts. *Acc. Chem. Res.* **2015**, *48*, 1494–1502.
- (3) (a) Campos, J. Bimetallic cooperation across the periodic table. *Nat. Rev. Chem.* **2020**, *4*, 696–702. (b) Powers, I. G.; Uyeda, C. Metal-metal bonds in catalysis. *ACS Catal.* **2017**, *7*, 936–958.
- (4) Buchwalter, P.; Rose, J.; Braunstein, P. Multimetallic Catalysis Based on Heterometallic Complexes and Clusters. *Chem. Rev.* **2015**, *115*, 28–126.
- (5) Paparo, A.; Okuda, J. Carbon Dioxide Complexes: Bonding Modes and Synthetic Methods. *Coord. Chem. Rev.* **2017**, *334*, 136–149.
- (6) (a) Burkart, M. D.; Hazari, N.; Tway, C. L.; Zeitler, E. L. Opportunities and Challenges for Catalysis in Carbon Dioxide Utilization. *ACS Catal.* **2019**, *9*, 7937–7956. (b) Appel, A. M.; Bercaw, J. E.; Bocarsly, A. B.; Dobbek, H.; Dubois, D. L.; Dupuis, M.; Ferry, J. G.; Fujita, E.; Hille, R.; Kenis, P. J. A. Frontiers, Opportunities, and Challenges in Biochemical and Chemical Catalysis of CO<sub>2</sub> Fixation. *Chem. Rev.* **2013**, *113*, 6621–6658.
- (7) Gibson, D. H. The Organometallic Chemistry of Carbon Dioxide. *Chem. Rev.* **1996**, *9*, 2063–2095.
- (8) (a) Gambarotta, S.; Arena, F.; Floriani, C.; Zanazzi, P. F. Carbon dioxide fixation: bifunctional complexes containing acidic and basic sites working as reversible carriers. *J. Am. Chem. Soc.* **1982**, *104*, 5082–5092. (b) Fachinetti, G.; Floriani, C.; Zanazzi, P. F. Bifunctional activation of carbon dioxide. Synthesis and structure of a reversible carbon dioxide carrier. *J. Am. Chem. Soc.* **1978**, *100*, 7405–7407.
- (9) (a) Hanna, T. A.; Baranger, A. M.; Bergman, R. G. Reaction of Carbon Dioxide and Heterocumulenes with an Unsymmetrical Metal–Metal Bond - Direct Addition of Carbon-Dioxide across a Zirconium–Iridium Bond and Stoichiometric Reduction of Carbon Dioxide to Formate. *J. Am. Chem. Soc.* **1995**, *117*, 11363–11364. (b) Krogman, J. P.; Foxman, B. M.; Thomas, C. M. Activation of CO<sub>2</sub> by a Heterobimetallic Zr/Co Complex. *J. Am. Chem. Soc.* **2011**, *133*, 14582–14585. (c) Mömning, C. M.; Otten, E.; Kehr, G.; Fröhlich, R.; Grimme, S.; Stephan, D. W.; Erker, G. Reversible Metal-Free Carbon Dioxide Binding by Frustrated Lewis Pairs. *Angew. Chem., Int. Ed.* **2009**, *48*, 6643–6646. (d) Schlenker, K.; Christensen, E. G.; Zhanserkeev, A. A.; McDonald, G. R.; Yang, E. L.; Lutz, K. T.; Steele, R. P.; Vanderlinden, R. T.; Saouma, C. T. Role of Ligand-Bound CO<sub>2</sub> in the Hydrogenation of CO<sub>2</sub> to Formate at a (PNP)Mn Catalyst. *ACS Catal.* **2021**, *11*, 8358–8369. (e) Escomel, L.; Del Rosal, I.; Maron, L.; Jeanneau, E.; Veyre, L.; Thieuleux, C.; Camp, C. Strongly Polarized Iridium<sup>δ-</sup>–Aluminum<sup>δ+</sup> Pairs: Unconventional Reactivity Patterns Including CO<sub>2</sub> Cooperative Reductive Cleavage. *J. Am. Chem. Soc.* **2021**, *143*, 4844–4856.
- (10) (a) Dobbek, H.; Svetlitchnyi, V.; Gremer, L.; Huber, R.; Meyer, O. Crystal Structure of a Carbon Monoxide Dehydrogenase Reveals a [Ni-4Fe-5S] Cluster. *Science* **2001**, *293*, 1281–1285. (b) Mankad, N. P.; Ghosh, D. Biomimetic Studies of the Mo/Cu Active Site of CO Dehydrogenase. *Comprehensive Coordination Chemistry III*, **2021**, pp 772–789.
- (11) Karunananda, M. K.; Mankad, N. P. Cooperative Strategies for Catalytic Hydrogenation of Unsaturated Hydrocarbons. *ACS Catal.* **2017**, *7*, 6110–6119.
- (12) (a) Agarwal, J.; Fujita, E.; Schaefer, H. F., III; Muckerman, J. T. Mechanisms for CO Production from CO<sub>2</sub> Using Reduced Rhenium Tricarbonyl Catalysts. *J. Am. Chem. Soc.* **2012**, *134*, 5180–5186. (b) Liu, L.; Cao, L. L.; Shao, Y.; Ménard, G.; Stephan, D. W. A Radical Mechanism for Frustrated Lewis Pair Reactivity. *Chem.* **2017**, *3*, 259–267. (c) Dasgupta, A.; Richards, E.; Melen, R. L. Frustrated Radical Pairs: Insights from EPR Spectroscopy. *Angew. Chem., Int. Ed.* **2021**, *60*, 53–65. (d) Holtrop, F.; Jupp, A.; Slootweg, J. C. Radicals in frustrated Lewis pair chemistry. *Springer, Cham*, **2021**, pp. 361–385.
- (13) (a) Charles III, R. M.; Brewster, T. P. H<sub>2</sub> and carbon-heteroatom bond activation mediated by polarized heterobimetallic complexes. *Coord. Chem. Rev.* **2021**, *433*, 213765. (b) Hicken, A.; White, A. J. P.; Crimmin, M. R. Selective Reduction of CO<sub>2</sub> to a Formate Equivalent with Heterobimetallic Gold–Copper Hydride Complexes. *Angew. Chem., Int. Ed.* **2017**, *56*, 15127–15130. (c) Mankad, N. P. Selectivity Effects in Bimetallic Catalysis. *Chem. - Eur. J.* **2016**, *22*, 5822–5829. (d) Bagherzadeh, S.; Mankad, N. P. Catalyst Control of Selectivity in CO<sub>2</sub> Reduction Using a Tunable Heterobimetallic Effect. *J. Am. Chem. Soc.* **2015**, *137*, 10898–10901. (e) Chipman, J. A.; Berry, J. F. Paramagnetic Metal–Metal Bonded Heterobimetallic Complexes. *Chem. Rev.* **2020**, *120*, 2409–2447. (f) Power, P. P. Main-group elements as transition metals. *Nature* **2010**, *463*, 171–177.
- (14) Nikonov, G. I. New Tricks for an Old Dog: Aluminum Compounds as Catalysts in Reduction Chemistry. *ACS Catal.* **2017**, *7*, 7257–7266.
- (15) (a) Lai, Q.; Bhuvanesh, N.; Ozerov, O. V. Unexpected B/Al Transmetalation within a Rh Pincer Complex. *J. Am. Chem. Soc.* **2020**, *142*, 20920–20923. (b) Hara, N.; Saito, T.; Semba, K.; Kuriakose, N.; Zheng, H.; Sakaki, S.; Nakao, Y. Rhodium Complexes Bearing PAIP Pincer Ligands. *J. Am. Chem. Soc.* **2018**, *140*, 7070–7073. (c) Ekkert, O.; White, A. J. P.; Toms, H.; Crimmin, M. R. Addition of Aluminium, Zinc and Magnesium Hydrides to Rhodium(III). *Chem. Sci.* **2015**, *6*, 5617–5622.
- (16) Anand, B. N.; Krossing, I.; Nöth, H. Synthesis and X-Ray Crystal Structure of (Tmp)<sub>2</sub>Al–Fe(Cp)(CO)<sub>2</sub>: An Alanil-Containing Iron Complex with a Tricoordinated Aluminum Atom. *Inorg. Chem.* **1997**, *36*, 1979–1981.
- (17) Braunschweig, H.; Müller, J.; Ganter, B. Molecular Structure of [CpFe(CO)<sub>2</sub>]<sub>2</sub>AlAr (Ar = 2-(Dimethylamino)methyl]phenyl): An Alanediyl Complex with Two Fe–Al Bonds. *Inorg. Chem.* **1996**, *35*, 7443–7444.
- (18) Mears, K. L.; Stennett, C. R.; Taskinen, E. K.; Knapp, C. E.; Carmalt, C. J.; Tuononen, H. M.; Power, P. P. Molecular Complexes Featuring Unsupported Dispersion-Enhanced Aluminum–Copper and Gallium–Copper Bonds. *J. Am. Chem. Soc.* **2020**, *142*, 19874–19878.

- (19) Liu, H.-Y.; Schwamm, R. J.; Hill, M. S.; Mahon, M. F.; McMullin, C. L.; Rajabi, N. A. Ambiphilic Al-Cu Bonding. *Angew. Chem., Int. Ed.* **2021**, *60*, 14390–14393.
- (20) Rudd, P. A.; Liu, S.; Gagliardi, L.; Young, V. G.; Lu, C. C. Metal-Alane Adducts with Zero-Valent Nickel, Cobalt, and Iron. *J. Am. Chem. Soc.* **2011**, *133*, 20724–20727.
- (21) Kong, R. Y.; Crimmin, M. R. *Dalton Trans.*, **2021**, *50*, 7810–7817.
- (22) (a) Fischer, R. A.; Priermeier, T. Transition-Metal-Substituted Alanes: Synthesis and Spectroscopic Studies and the Structure of  $(\eta^5\text{-C}_5\text{H}_5)(\text{CO})_2\text{Fe-Al}[(\text{CH}_2)_3\text{NMe}_2](\text{tBu})$ . *Organometallics* **1994**, *13*, 4306–4314. (b) Jones, C.; Aldridge, S.; Gans-Eichler, T.; Stasch, A. Synthesis and characterisation of complexes of Group 13 metal amidinate heterocycles with the  $\text{CpFe}(\text{CO})_2$  fragment. *Dalton Trans.* **2006**, 5357–5361. (c) Riddlestone, I. M.; Urbano, J.; Phillips, N.; Kelly, M. J.; Vidovic, D.; Bates, J. I.; Taylor, R.; Aldridge, S. Salt Metathesis for the Synthesis of M-Al and M-H-Al Bonds. *Dalton Trans.* **2013**, *42*, 249–258.
- (23) Whiteoak, C. J.; Kielland, N.; Laserna, V.; Escudero-Adán, E. C.; Martin, E.; Kleij, A. W. A Powerful Aluminum Catalyst for the Synthesis of Highly Functional Organic Carbonates. *J. Am. Chem. Soc.* **2013**, *135*, 1228–1231.
- (24) Hicks, J.; Mansikkamäki, A.; Vasko, P.; Goicoechea, J. M.; Aldridge, S. A Nucleophilic Gold Complex. *Nat. Chem.* **2019**, *11*, 237–241.
- (25) Warratz, S.; Postigo, L.; Royo, B. Direct Synthesis of Iron(0) *N*-Heterocyclic Carbene Complexes by Using  $\text{Fe}_3(\text{CO})_{12}$  and Their Application in Reduction of Carbonyl Groups. *Organometallics* **2013**, *32*, 893–897.
- (26) Lamb, J. R.; Hubbell, A. K.; MacMillan, S. N.; Coates, G. W. Carbonylative, Catalytic Deoxygenation of 2,3-Disubstituted Epoxides with Inversion of Stereochemistry: An Alternative Alkene Isomerization Method. *J. Am. Chem. Soc.* **2020**, *142*, 8029–8035.
- (27) Hirano, M.; Akita, M.; Tani, K.; Kumagai, K.; Kasuga, N. C.; Fukuoka, A.; Komiyama, S. Activation of Coordinated Carbon Dioxide in  $\text{Fe}(\text{CO})_2(\text{Depe})_2$  by Group 14 Electrophiles. *Organometallics* **1997**, *16*, 4206–4213.
- (28) Friedrich, H. B.; Onani, M. O.; Rademeyer, M. Bromopropylideneiron( $\eta^5$ -pentamethyl-cyclopentadienyl)iron(II). *Acta Cryst. E* **2004**, *60*, m551–m553.
- (29) Chu, T.; Vyboishchikov, S. F.; Gabidullin, B.; Nikonov, G. I. Oxidative Cleavage of C = S and P = S Bonds at an AlI Center: Preparation of Terminally Bound Aluminum Sulfides. *Angew. Chem., Int. Ed.* **2016**, *55*, 13306–13311.
- (30) Jancik, V.; Roesky, H. W.; Neculai, D.; Neculai, A. M.; Herbst-Irmer, R. Preparation of  $[\text{LAl}(\mu\text{-S})_2\text{MCP}_2]$  (M = Ti, Zr) from the Structurally Characterized Lithium Complexes  $[\{\text{LAl}(\text{SH})\{\text{SLi}(\text{thf})_2\}\}]$  and  $[\{\text{LAl}(\{\text{SLi}(\text{thf})_2\})_2\}]\cdot 2\text{THF}$ . *Angew. Chem., Int. Ed.* **2004**, *43*, 6192–6196.
- (31) Ramalakshmi, R.; Maheswari, K.; Sharmila, D.; Paul, A.; Roisnel, T.; Halet, J.-F.; Ghosh, S. Reactivity of cyclopentadienyl transition metal(II) complexes with borate ligands: Structural characterization of the toluene-activated molybdenum complex  $[\text{Cp}^*\text{Mo}(\text{CO})_2(\eta^3\text{-CH}_2\text{C}_6\text{H}_5)]$ . *Dalton Trans.* **2016**, *45*, 16317–16324.
- (32) Bitterwolf, T. E. Photochemistry and Reaction Intermediates of the Bimetallic Group VIII Cyclopentadienyl Metal Carbonyl Compounds,  $(\eta^5\text{-C}_5\text{H}_5)_2\text{M}_2(\text{CO})_4$  and Their Derivatives. *Coord. Chem. Rev.* **2000**, *206–207*, 419–450.
- (33) Cotton, F. A.; Troup, J. M. Accurate determination of a classic structure in the metal carbonyl field: nonacarbonyl-di-iron. *J. Chem. Soc., Dalton Trans.* **1974**, 800–802.
- (34) Mitschler, A.; Rees, B.; Lehmann, M. S. Electron Density in Bis(dicarbonyl- $\pi$ -cyclopentadienyl)iron at Liquid Nitrogen Temperature by X-Ray and Neutron Diffraction. *J. Am. Chem. Soc.* **1978**, *100*, 3390–3397.
- (35) Giannini, L.; Solari, E.; Angelis, S. D.; Ward, T. R.; Floriani, C.; Chiesi-Villa, A.; Rizzoli, C. Migratory Aptitude of the Zr-C Functionalities Bonded to a Macrocyclic Structure: Thermally- and Solvent-assisted Intra- and Intermolecular Migrations in Dialkyl(dibenzotetramethyltetraazaannulene)zirconium(IV). *J. Am. Chem. Soc.* **1995**, *117*, 5801–5811.
- (36) (a) Foster, J. P.; Weinhold, F. Natural hybrid orbitals. *J. Am. Chem. Soc.* **1980**, *102*, 7211–7218. (b) Reed, A. E.; Weinhold, F. Natural bond orbital analysis of near-Hartree-Fock water dimer. *J. Chem. Phys.* **1983**, *78*, 4066–4073.
- (37) (a) Bader, R. F. W. A quantum theory of molecular structure and its applications. *Chem. Rev.* **1991**, *91*, 893–928. (b) Bader, R. F. W. Atoms in Molecules. A Quantum Theory (Oxford Univ. Press, Oxford, **1994**).
- (38) Laidig, K. E.; Bader, R. F. W. Properties of Atoms in Molecules: Atomic Polarizabilities. *J. Chem. Phys.* **1990**, *93*, 7213–7224.
- (39) Jayarathne, U.; Mazzacano, T. J.; Bagherzadeh, S.; Mankad, N. P. Heterobimetallic Complexes with Polar, Unsupported Cu-Fe and Zn-Fe Bonds Stabilized by *N*-Heterocyclic Carbenes. *Organometallics* **2013**, *32*, 3986–3992.
- (40) (a) Wiberg, K. B. Application of the pople-santry-segal CNDO method to the cyclopropylcarbonyl and cyclobutyl cation and to bicyclobutane. *Tetrahedron* **1968**, *24*, 1083–1096. (b) Sizova, O. V.; Skripnikov, L. V.; Sokolov, A. Y. Symmetry decomposition of quantum chemical bond orders. *J. Mol. Struct. (Theochem)* **2008**, *870*, 1–3, 1–9.
- (41) González-Fabra, J.; Castro-Gómez, F.; Sameera, W. M. C.; Nyman, G.; Kleij, A. W.; Bo, C. Entropic Corrections for the Evaluation of the Catalytic Activity in the Al(III) Catalysed Formation of Cyclic Carbonates from  $\text{CO}_2$  and Epoxides. *Catal. Sci. Technol.* **2019**, *9*, 5433–5440.
- (42) Tanaka, R.; Yamashita, M.; Chung, L. W.; Morokuma, K.; Nozaki, K. Mechanistic Studies on the Reversible Hydrogenation of Carbon Dioxide Catalyzed by an Ir-PNP Complex. *Organometallics* **2011**, *30*, 6742–6750.
- (43) John R. Pinkes; Christopher J. Masi; Robert Chiulli; Bryan D. Steffey; Cutler, A. R. Carbon Dioxide Complexation: Infrared Spectroscopy of Iron and Ruthenium  $\eta^5$ -Cyclopentadienyl Carbonyl Metallocarboxylates. *Inorg. Chem.* **1997**, *36*, 70–79.
- (44) Castro-Rodríguez, I.; Nakai, H.; Zakharov, L. N.; Rheingold, A. L.; Meyer, K. A linear, O-Coordinated  $\eta^1\text{-CO}_2$  Bound to Uranium. *Science* **2004**, *305*, 1757–1759.
- (45) Saouma, C. T.; Lu, C. C.; Day, M. W.; Peters, J. C.  $\text{CO}_2$  reduction by Fe(I): solvent control of C–O cleavage versus C–C coupling. *Chem. Sci.* **2013**, *4*, 4042–4051.
- (46) Falconer, R. L.; Nichol, G. S.; Smolyar, I. V.; Cockroft, S. L.; M. J. Cowley. Reversible Reductive Elimination in Aluminum(II) Dihydrides. *Angew. Chem. Int. Ed.* **2021**, *60*, 2047–2052.
- (47) (a) Adamo, C.; Barone, V. Toward reliable density functional methods without adjustable parameters: The PBE0 model. *J. Chem. Phys.* **1999**, *110*, 6158–6169. (b) Grimme, S.; Ehrlich, S.; Goerigk, L. Effect of the damping function in dispersion corrected density functional theory. *J. Comp. Chem.* **2011**, *32*, 1456–1465. (c) Weigend, F.; Ahlrichs, R. Balanced basis sets of split valence, triple zeta valence and quadruple zeta valence quality for H to Rn: Design and assessment of accuracy. *Phys. Chem. Chem. Phys.* **2005**, *7*, 3297–3305. (d) Marenich, A. V.; Cramer, C. J.; Truhlar, D. G.; Universal solvation model based on solute electron density and a continuum model of the solvent defined by the bulk dielectric constant and atomic surface tensions. *J. Phys. Chem. B* **2009**, *113*, 6378–6396.
- (48) Gaussian 16, Revision B.01, Frisch, M. J.; Trucks, G. W.; Schlegel, H. B.; Scuseria, G. E.; Robb, M. A.; Cheeseman, J. R.; Scalmani, G.; Barone, V.; Petersson, G. A.; Nakatsuji, H.; Li, X.; Caricato, M.; Marenich, A. V.; Bloino, J.; Janesko, B. G.; Gomperts, R.; Menucci, B.; Hratchian, H. P.; Ortiz, J. V.; Izmaylov, A. F.; Sonnenberg, J. L.; Williams-Young, D.; Ding, F.; Lipparini, F.; Egidi, F.; Goings, J.; Peng, B.; Petrone, A.; Henderson, T.; Ranasinghe, D.; Zakrzewski, V. G.; Gao, J.; Rega, N.; Zheng, G.; Liang, W.; Hada, M.; Ehara, M.; Toyota, K.; Fukuda, R.; Hasegawa, J.; Ishida, M.; Nakajima, T.; Honda, Y.; Kitao, O.; Nakai, H.; Vreven, T.; Throssell, K.; Montgomery, J. A., Jr.; Peralta, J. E.; Ogliaro, F.; Bearpark, M. J.; Heyd, J. J.; Brothers, E. N.; Kudin, K. N.; Staroverov, V. N.; Keith, T. A.; Kobayashi, R.; Normand, J.; Raghavachari, K.; Rendell, A. P.; Burant, J. C.; Iyengar, S. S.; Tomasi, J.; Cossi, M.; Millam, J. M.; Klene, M.; Adamo, C.; Cammi, R.; Ochterski, J. W.; Martin, R. L.; Morokuma, K.; Farkas, O.; Foresman, J. B.; Fox, D. J. Gaussian, Inc., Wallingford CT, **2016**.

(49) NBO Version 3.1, Glendening, E. D.; Reed, A. E.; Carpenter, J. E.; Weinhold, F.

(50) Lu, T.; Chen, F. Multiwfn: A Multifunctional Wavefunction Analyzer. *J. Comput. Chem.* **2012**, *33*, 580–592.

